Design Procedure for a Novel LMDS Base Station Reflectarray Antenna

Reza Masoumi ⓘ, Robab Kazemi ⓘ *

Faculty of Electrical and Computer Engineering, University of Tabriz, Tabriz, Iran

ABSTRACT: A Reflectarray Antenna is designed to operate at X-band as a Local Multipoint Distribution Service (LMDS) base station antenna. It is a center-fed single layer reflectarray consisting of 23×27 elements. The unit cell of the reflectarray has linear polarization with more than 400° linear phase shift and its geometrical parameters have been optimized to achieve wide bandwidth and low cross polarization (XP) level for the reflectarray. An iterative design procedure, that is valid for obtaining any arbitrary pattern, has been implemented to achieve the specified radiation pattern over a desired frequency range. The method has been successfully applied to a LMDS base station antenna, characterized by a sectorial cosecant squared beam in the frequency range of 9.3 GHz - 11.5 GHz. The simulation results are in a good agreement with the design requirements. The antenna has cosecant squared pattern over the bandwidth of 21%, XP level better than -30 dB, and SLL less than -20 dB in both elevation and azimuth planes. The total size of the 23×27-element array is 246×289 mm2, and its 1dB gain bandwidth is wider than 19%. The proposed antenna performs significantly better than similar structures and has all the features and standards required for LMDS base station antenna.

1- Introduction

Reflectarray Antennas (RAs) are preferred in phased array antennas, especially in telecommunication satellites and beam-shaping applications [1-3] due to their planar geometry, low profile, low manufacturing cost, low weight, ease of transportation and capability to beamforming and control. However, the main deficiency of reflectarrays is their narrow bandwidth due to the intrinsic finite bandwidth of microstrip elements [4]. Therefore, in recent decades, various structures of RAs have been introduced in the literature, and the bandwidth issue has been resolved to some extent [5, 6].

There are several methods to increase the bandwidth of RAs, including: 1) using multilayer structures, which may substantially increase the cost and complexity of the manufacturing process and increase the weight and loss; 2) utilizing thicker substrates, which decreases the phase variation capability due to the reduction of phase response slope, thus reduces the efficiency; 3) using phase delay lines to obtain a phase range much larger than 360°; 4) employing multi-band antennas [5-7].

In recent years, many efforts have been made to achieve beam-shaping reflectarrays [8-11]. In [8], a folded multi-layer microstrip reflectarray with shaped pattern is presented. In [9], a phase-only algorithm is used to obtain required phase shift on a large Reflectarray Antenna surface. In [10],

a multiple-beam sector antenna with dual planar reflectarray is proposed. A dual planar reflectarray with synthesized phase and amplitude distribution, producing multi-beam, is studied in [11]. However, their beam shaping is restricted to specific patterns and the design process depends on various parameters, which require simultaneous optimization.

In this paper, we proposed a novel unit cell with a symmetric configuration which provides appropriate phase variation to design a beam-shaping reflectarray for efficient operation in LMDS base stations. The unit cell is comprised of a cross-shaped slot at the center of a square ring, four square slots at the corners and four rectangular stubs connected to the middle of the main square sides. This unit cell provides a phase variation larger than 360°. In addition, the geometrical parameters of the unit cell are optimized to increase the bandwidth and achieve appropriate co- and cross-polarization components of the radiation patterns at both elevation and azimuth planes. At the next step, a phase-related synthesis method is applied to obtain the required phase-shift on the reflectarray surface, characterized by a sectorial Cosecant squared beam in the frequency range of 9.3 GHz-11.5 GHz.

The paper is organized as follows: In Section 2, the design procedure of the RA unit cell is presented. Phase distribution of RA and numerical results are discussed and compared to a similar antenna in section 3. Finally, the conclusion is given in section 4.

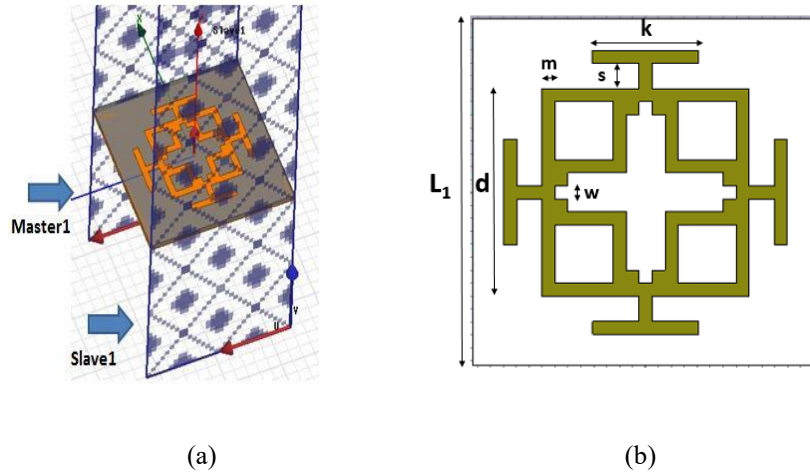*Corresponding author's email: r.kazemi@tabrizu.ac.ir

21

(a)   (b)

Fig. 1. (a) The novel unit cell of the RA modeled in HFSS, (b) parameters of the unit cell

Table 1. Optimized dimensions of the unit cell

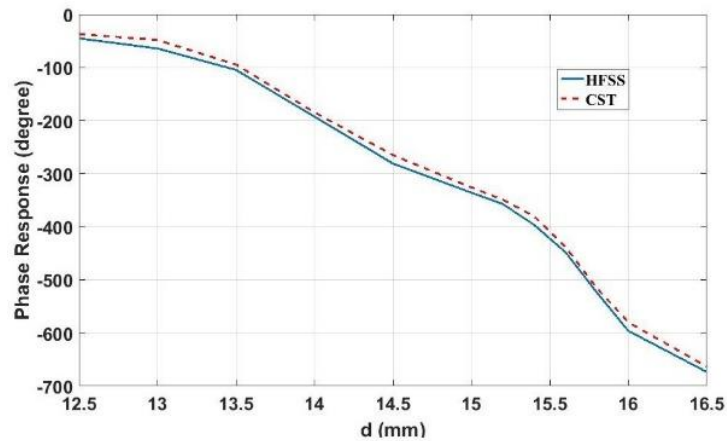| Parameter	m	w	k	s	L_1
Value (mm)	1	1	8.15	1.95	20.7

Fig. 2. The optimized unit cell phase response simulated in HFSS and CST

2- Design Procedure of the Unit Cell

The proposed unit cell of RA is comprised of a cross-shaped slot at the center of a square ring, four square slots at the corners and four rectangular stubs connected to the middle of the main square sides, as shown in Fig. 1. This configuration produces adequate phase shift, which is achieved by changing the length of the main square side "d".

The ring size and stub lengths are optimized in both HFSS and CST simulation softwares with master-slave and unit cell boundary conditions, respectively. The unit cell is designed on RO4003C substrate with the thickness of 0.813 mm, ε_r =3.55, and $\tan\delta$ = 0.0027. Its dimensions are optimized for appropriate bandwidth and low cross-polarization, and are summarized in Table 1.
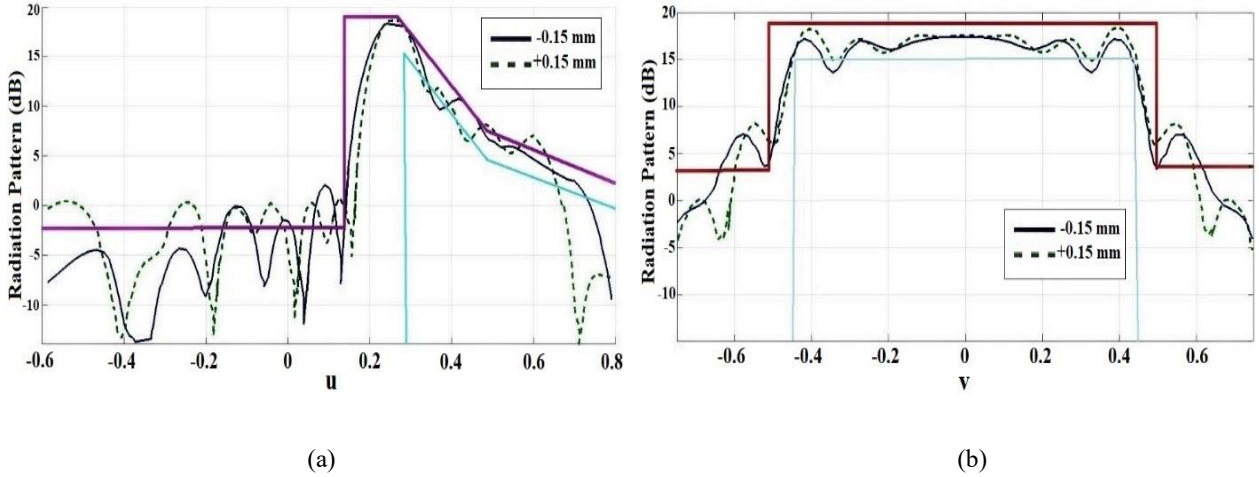
(a)   (b)

Fig. 3. Radiation patterns of the RA with ±0.15mm tolerance at a) φ=0° plane, b) φ=90° plane

The optimized phase response of the unit cell is shown in Fig. 2. As shown, a smooth and linear phase shift with larger than 360° coverage is achieved. However, the tolerance of the RA characteristics against the design errors should be investigated as well. For this purpose, the largest variation of parameters of the unit cell, "±ΔL", in which the radiation pattern of RA still in the desired shape, is calculated. The linearity of the phase shift and its wider phase response range confirm the tolerance of the structure against design errors. In this case, the maximum tolerance of the RA is ΔL = ± 0.15 mm which is easily accomplished by current fabrication technologies. The predicted radiation patterns of RA with ±0.15mm tolerance are calculated in elevation (φ=0°) and azimuth (φ=90°) planes and shown in Fig. 3.

3- Phase Distribution of RA

The best phase distribution on the RA surface is obtained through an iterative approach for both elevation and azimuth planes simultaneously. First, a 3160-07 standard model of feed horn, which its radiation pattern is usually modeled as $Cos^q(\theta)$, is designed in a way that its efficiency (the product of illumination and spill-over efficiencies) has the maximum value at the center frequency of f_0 = 10.4 GHz. This horn antenna, with dimensions of Table 2, is located at a distance of 50 mm from the RA surface.

The feed horn, its simulated radiation pattern at $f_0 = 10.4$ GHz and the variation of the peak gain over the frequency range is illustrated in Fig. 4.

At the second step, the required phase shift for each element of the RA is calculated to produce a plane wave. The phase shifts should compensate the difference in spatial phase delays between the feed and each element of RA. RA is illuminated by the horn feed located at a distance of r_f from the reflectarray surface. The required phase delay for each element is calculated as [1]:

$$\alpha_{mn} - k_0 \left[\left| \vec{r}_{mn} - \vec{r}_f \right| - \vec{r}_{mn} \hat{u}_0 \right] = 2n\pi, \quad (m,n) = 0,1,2,... \tag{1}$$

According to Fig. 5, α_{mn} is the required phase shift for (m,n)th element, $\vec{r}_{mn}$ is the position vector of the (m,n)th element, and $\hat{u}_0$ is the direction of the main beam in the free-space. In fact, Equation (1) results in a co-phase plane for the reflected wave. The reflected field in the observation direction of $\hat{u}$ at the farfield is calculated by the array theory [1]:

Table 2. Physical dimensions of the feed horn"

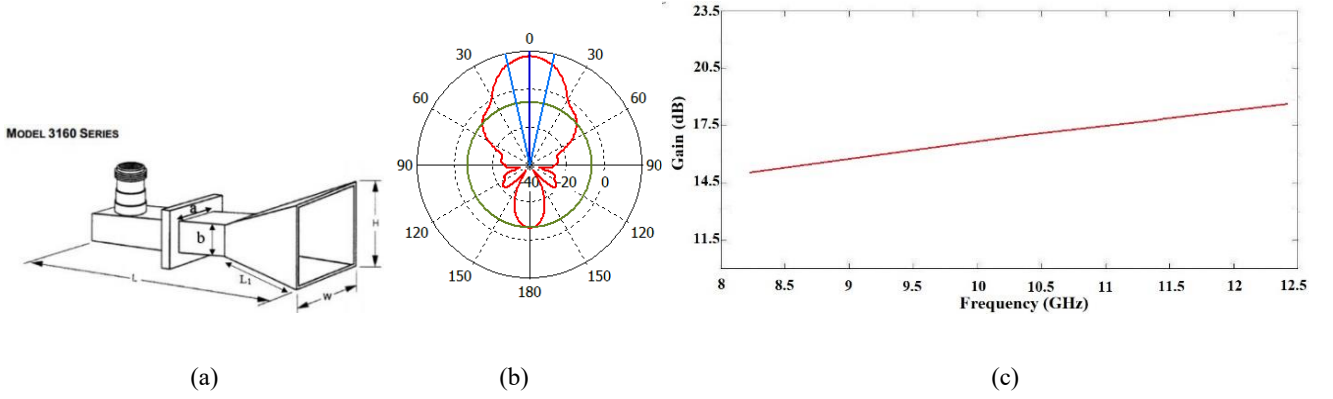| Model	Waveguide a × b (cm²)	Bandwidth (GHz)	H (cm)	W (cm)	L (cm)	L1 (cm)
3160-07	2.286×1.016	8-12	7.6	5.8	22.9	12.62

(a)   (b)   (c)

Fig. 4. (a) X-band feed horn schematic, (b) radiation pattern at f0 =10.4GHz, (c) variation of peak gain vs. frequency

$$E(\hat{u}) = \sum_{m=1}^{M}\sum_{n=1}^{N} F(\vec{r}_{mn}.\vec{r}_f)A(\vec{r}_{mn}.\hat{u}_0)$$

$$A(\hat{u}.\hat{u}_0) \times e^{(-jk_0[|\vec{r}_{mn}-\vec{r}_f|-\vec{r}_{mn}.\hat{u}_0]+j\alpha_{mn})} \quad (2)$$

where F and A are the radiation patterns of the feed and the unit cell, respectively. In the third step and beam-shaping process, first a large q is considered for the radiation pattern of the horn feed. With this high tapering (q), only the central elements of RA receive most of the radiated power from the horn. Next, the radiation patterns in elevation and azimuth planes are considered to be superposition of pencil beams having different main lobe direction (θ_s). Using Fast Fourier Transform (FFT), the phases are calculated and the desired beam shapes are achieved. For a 2D array, the array factor $F(\theta,\varphi)$ is calculated as [1]:

$$E(\hat{u}) = \sum_{m=1}^{M}\sum_{n=1}^{N} F(\vec{r}_{mn}.\vec{r}_f)A(\vec{r}_{mn}.\hat{u}_0)$$

$$A(\hat{u}.\hat{u}_0) \times e^{(-jk_0[|\vec{r}_{mn}-\vec{r}_f|-\vec{r}_{mn}.\hat{u}_0]+j\alpha_{mn})} \quad (3)$$

We define the parameter M as the total radiation patterns of all elements of the given array, and B as the combination of all the patterns that satisfy the requirements of predefined LMDS antenna (desired). These requirements are expressed as two horizontal and vertical masks which set the upper and lower limitations.

The intersection approach, which finds the similarities of the two M and B sets, is employed using successive projectors. Successive projector is an operator which gives the best approach to a goal function according to a presumed scale, such as mean square norm [1]. In this article, Fourier series gives the best mean square norm and is used as the basis of alternating projector method. The iteration begins
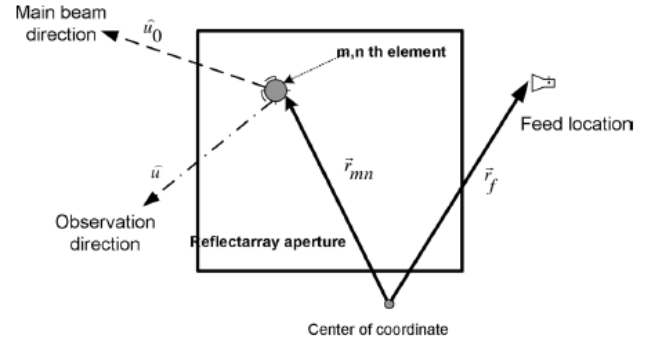

Fig. 5. Reflectarray coordinate system

with x_n and by using the projectors becomes x_{n+1} in each step as follows:

$$x_{n+1} = P_B P_M x_n \quad (4)$$

where P_B and P_M are projectors defined as follows according to the masks:

$$P_M F(u) = \begin{cases} M_U(u)\dfrac{F(u)}{|F(u)|} & |F(u)| > M_U(u) \\ F(u) & M_L(u) \le F(u) \le M_U(u) \\ M_L(u)\dfrac{F(u)}{|F(u)|} & |F(u)| < M_L(u) \end{cases} \quad (5)$$

M_L and M_U are the short form for the lower and upper masks, respectively, and P_M is a projector which changes the array factor in a way that fits on or between the masks. With small number of elements being involved at first, the array
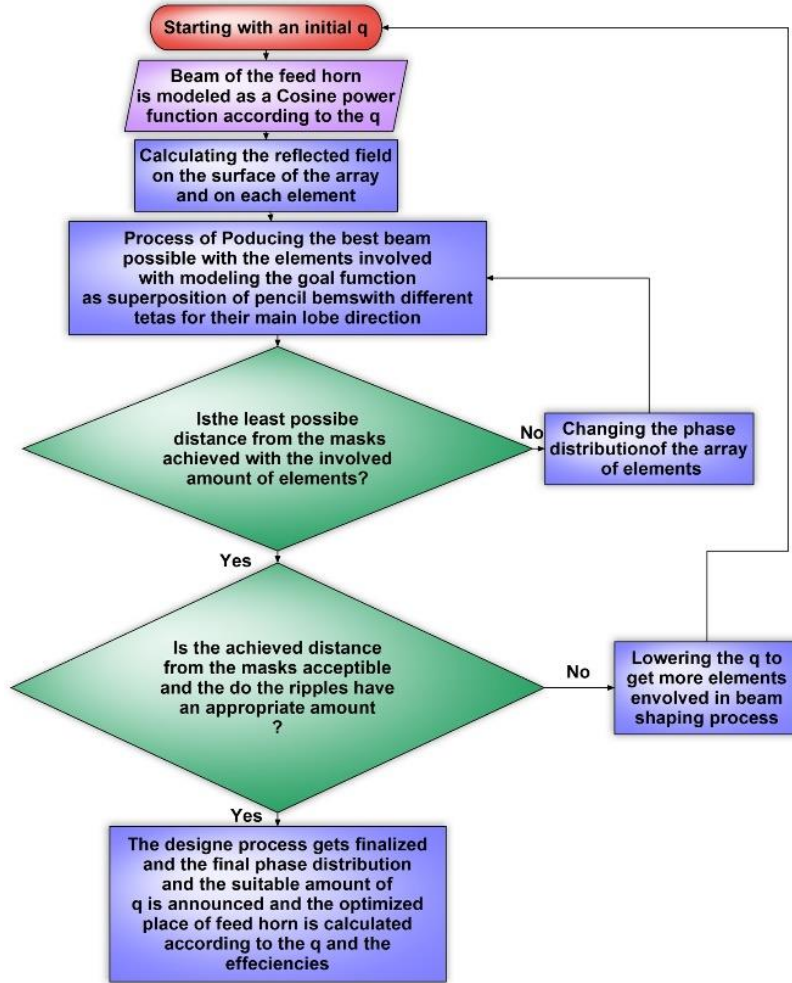
Fig. 6. Flow chart of design process

factor and element pattern is considered in shaping super-positioned beams. The phase distribution is acceptable in each step if the goal function, which is the difference from the masks in several points, gets minimum. Second, it is investigated whether the optimal achieved pattern serves the requirements of the masks and has an acceptable maximum ripple level. If with the primary q and related number of elements, the process converges to the optimal results, it is finished, if not, q becomes smaller and more elements are illuminated. The process continues until the produced patterns become acceptable with minimum number of elements and fit properly into the masks of cosecant squared beam in elevation and sectoral beam in azimuth planes. The flowchart of the design process is shown in Fig. 6. The phase distribution on array surface is achieved in an iterative process with increasing the number of elements being involved in shaping the pattern. The goal function for the design is defined as (6), which simultaneously reduces the side lobe level in the process of finding the best distribution to produce the pattern satisfying the requirements of the masks. w_1 and w_2 are the weighting coefficients for the main lobe and the side lobes, respectively.

$$
\begin{aligned}
Fitness = w_1 . \sum_{\substack{(u,v) \in mainbeam \\ and \ |E(u,v)| > M_L(u,v)}} \sum \left(|E(u,v) - M_L(u,v)| \right)^2 \\
+ w_2 . \sum_{\substack{(u,v) \in mainbeam \\ and \ |E(u,v)| < M_U(u,v)}} \sum \left(|E(u,v) - M_U(u,v)| \right)^2
\end{aligned}
\tag{6}
$$

Lowering the side lobe level can also be fulfilled by using special tapering on the phase distribution of the elements, like Chebyshev. The shapes of the acceptable masks for ETSI standards are shown in Fig. 7 for both planes with following transforms:

$$
v = sin\theta sin\varphi \ , \ u = sin\theta cos\varphi
\tag{7}
$$

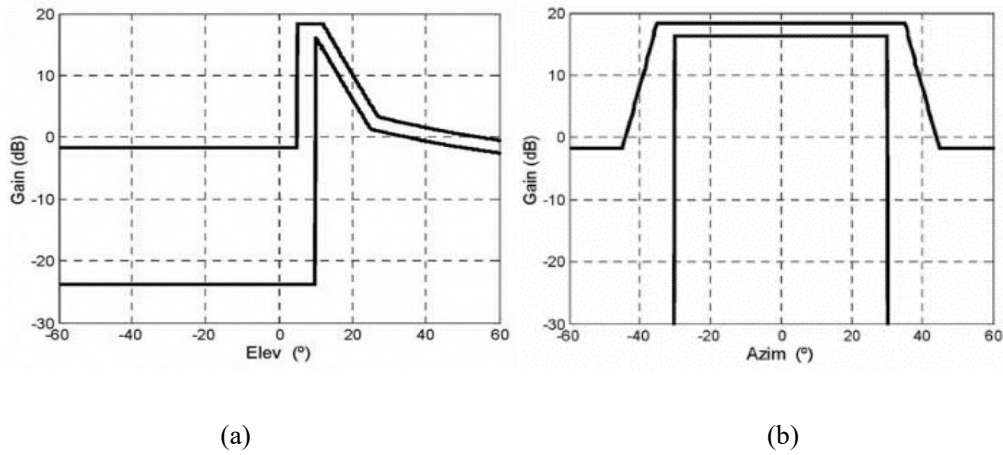(a)   (b)

Fig. 7. (a) Cosecant squared mask, (b) sectoral mask
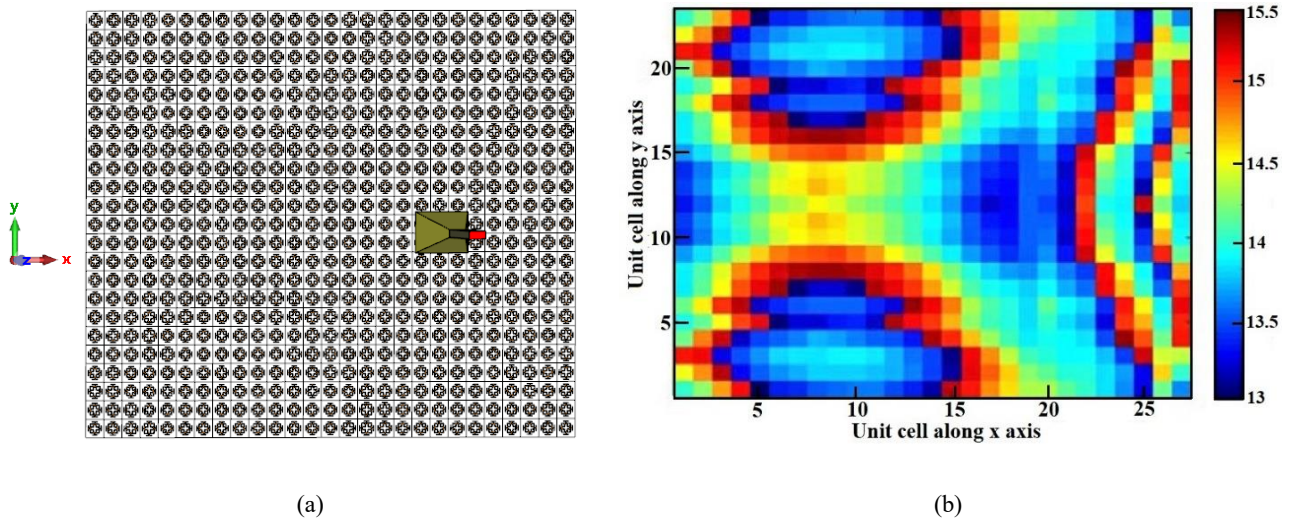

(a)   (b)

Fig. 8. (a) Lateral view of reflectarray, (b) phase distribution of elements on the surface of the RA

The proposed reflectarray and its feed horn are simulated in CST and shown in Fig. 8(a). The 23×27 unit cells form an array with a total size of 246×289 mm². In addition, the optimized phase distribution on the RA surface is illustrated in Fig. 8(b).

For covering 360° phase shift, the lengths of the unit cells are changed from 13 mm to 15.6 mm. Due to having the desired sectoral beam in azimuth plane, which is symmetric, the phase shift of the elements on the surface of the reflectarray is symmetric in *y*-direction as well. The radiation patterns of RA in elevation and azimuth planes are calculated analytically by using Matlab coding, and verified by CST full-wave simulator. The results are compared with the [12] in Fig. 9.

Having low cross-polarization (XP) level is one of the most important aspects of antenna design procedure. Smooth phase shift response of the designed unit cell, as well as appropriate phase distribution of the elements, result in low cross-polarization level. The XP patterns in elevation and azimuth planes for $f_0 = 10.4$ GHz are shown in Fig.10.

As can be seen, the XP level of the proposed RA is less than -30 dB, which approves the linear polarization of RA. The Co-pol and XP radiation patterns at the lower and upper edges of the bandwidth (9.3GHz and 11.5 GHz) in two orthogonal planes are plotted in Figs. 11 and 12, respectively. The XP level is less than -30dB all over the bandwidth. The radiation patterns show good fitting within the masks in the lower and upper edges of the desired frequency range.
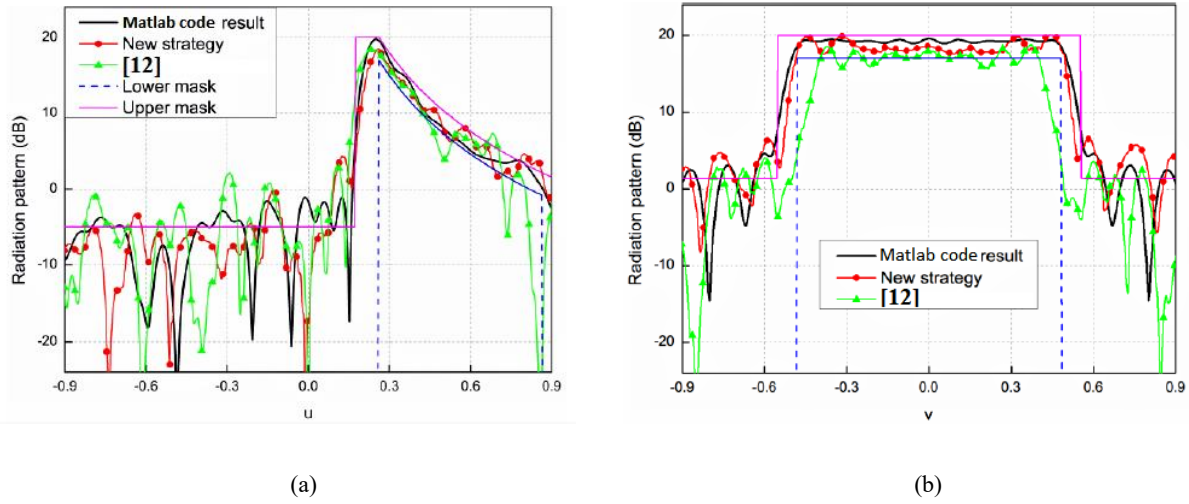
(a)   (b)

Fig. 9. Comparison of the radiation patterns of the proposed RA with [12] at f0 = 10.4 GHz; (a) φ=0° plane, (b) φ=90° plane
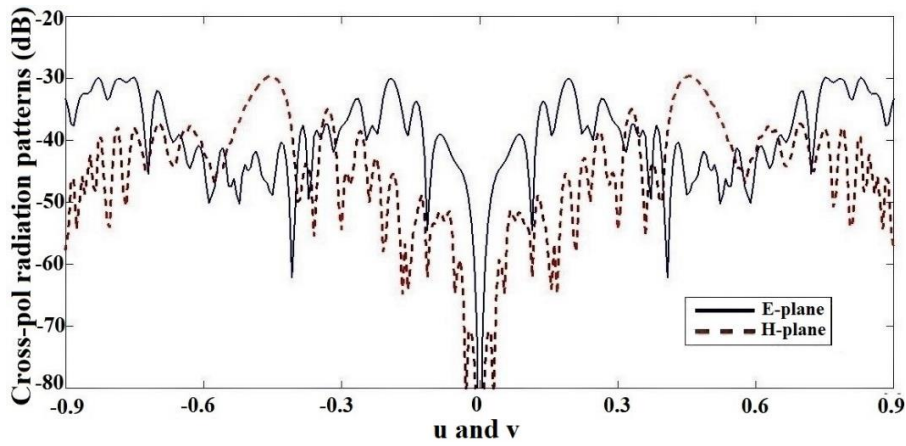

Fig. 10. XP level in elevation and azimuth planes at the center frequency of 10.4 GHz

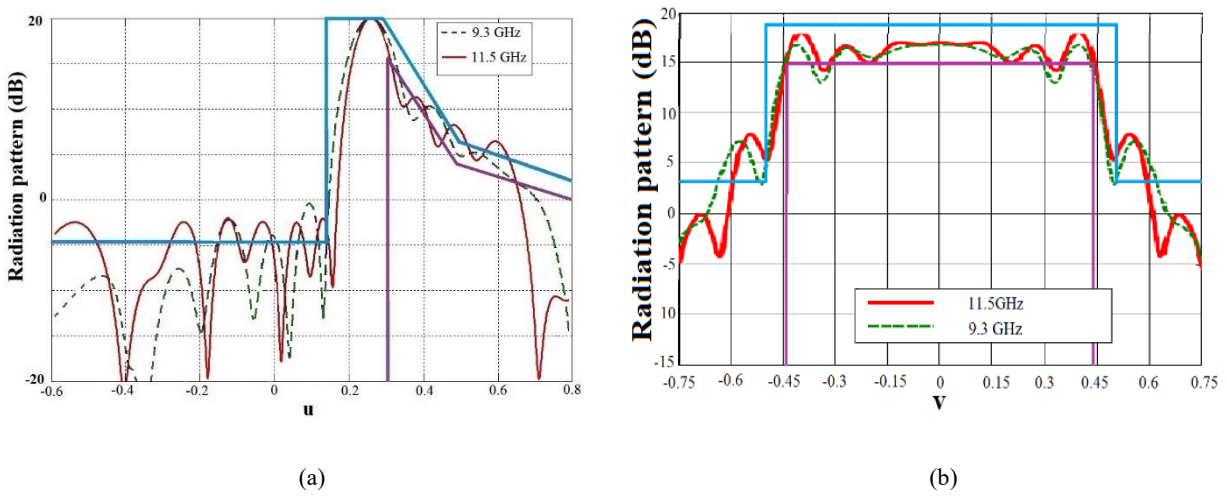(a)   (b)

Fig. 11. Co-pol radiation patterns at 9.3 GHz and 11.5 GHz; (a) at φ=0° plane, (b) at φ=90° plane
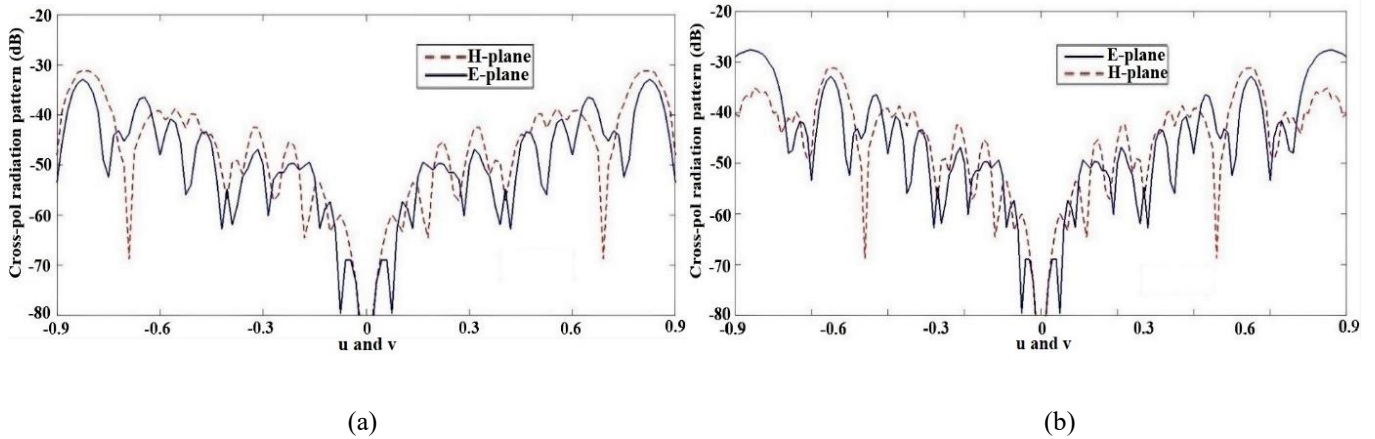
(a)

(b)

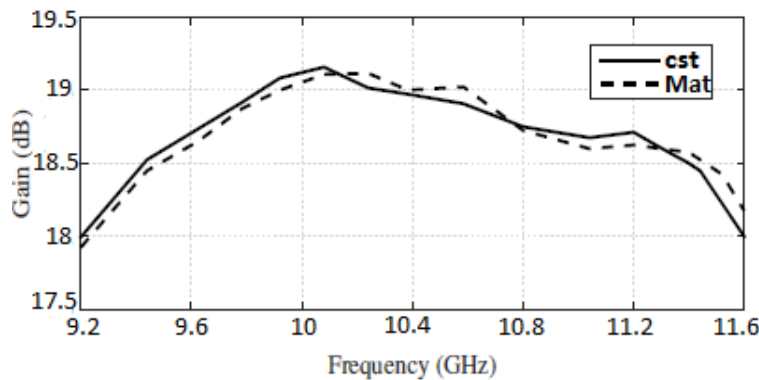**Fig. 12. Cross-polarization radiation patterns; (a) at 9.3 GHz, (b) at 11.5 GHz**

Fig. 13. Calculated and simulated peak gain vs. frequency

The variation of peak gain of the reflectarray vs. frequency is plotted in Fig.13. It is higher than 18dB at the range of 9.3 GHz - 11.5 GHz, and meets ETSI standards. Therefore, the proposed RA fulfills both desired radiation patterns and minimum acceptable gain requirements.

4- Conclusion

In this paper, a novel single-layer linearly polarized unit cell is proposed for Reflectarray Antennas, which has some unique features. The proposed unit cell is comprised of a cross-shaped slot at the center of a square ring, four square slots at the corners and four rectangular stubs connected to the middle of the main square sides. Its dimensions are optimized to obtain phase shift larger than 360° with smooth variation. A phase-related iterative synthesis method was acquired to calculate the appropriate phase shift on the reflectarray surface. A rectangular reflectarray of this proposed element is arranged in a 23×27 grid with a total size of 246×289 mm^2 to produce a Cosecant squared sectoral pattern. The demonstrated reflectarray has 21% bandwidth and perfectly meets the requirements of the LMDS base station antenna. The simulation results show that the structure has wider bandwidth and lower XP level compared to the similar works.

References

[1] J. Huang, J.A. Encinar, Reflectarray Antennas: theory, designs, and applications, Wiley-IEEE Press, (2018).

[2] E. Carrasco, J. Encinar, Y. Rahmat-Samii, Reflectarray Antennas: A review, Forum for Electromagnetic Research Methods and Application Technologies (FERMAT), 50 (2016).

[3] K. Narayanasany, G. Mohammed, K. Savarimuthu, A comprehensive analysis on the state-of-the-art developments in reflectarray, transmitarray, and transmit-Reflectarray Antennas, Int J RF Microw Comput Aided Eng, 30 (2020).

[4] M. H. Dahri, M. H. Jamaluddin, M. I. Abbasi, A Review of wideband Reflectarray Antennas for 5G communication

[5] Q. Gao, J. Wang, Y. Li, A multiresonant element for bandwidth enhancement of circularly polarized Reflectarray Antennas, IEEE Antennas and Wireless Propagation Letters, 17(5) (2018) 727-730.

[6] V. Suresh, G. Mohammed, K.Narayanasamy, A novel broadband reflectarray for 5G satellite communications, Int J RF Microw Comput Aided Eng, 32(2) (2022).

[7] M. Karimipour, N. Komjani, I. Aryanian, Broadband, dual-band reflectarray with dual orthogonal polarisation for single and multi-beam patterns, IET Microw. Antennas Propag., 13 (2018) 2037-2045.

[8] J. A. Zornoza, R. Leberer, J. A. Encinar, W. Menzel, Folded multilayer microstrip reflectarray with shaped pattern, IEEE Transactions on Antennas and Propagation, 54(2) (2006) 510-518.

[9] I.Aryanian, A.abdipour, Gh. Moradi, Design and efficient analysis of large Reflectarray Antenna, AUT Journal of Electrical Engineering, 46(1) (2014) 49-58.

[10] M. Thiel, W. Menzel, A multiple-beam sector antenna with a dual planar reflectarray arrangement, IEEE European Radar Conference, (2006) 53-56.

[11] R. Leberer, W. Menzel, A dual planar reflectarray with synthesized phase and amplitude distribution, IEEE Transactions on Antennas and Propagation, 53(11) (2005) 3534-3539.

[12] D. Prado, M. Arrebola, M. Pino, Improved reflectarray phase-only synthesis using the generalized intersection approach with dielectric frame and first principle of equivalence, International Journal of Antennas and Propagation, 6 (2017) 1-11.